



Magnetic Resonant Pulsed Pumping of Rubidium

by

Adam Newton Wright

Submitted in Partial Fulfillment of the
Requirements for the Degree

Bachelor of Arts

Supervised by
Dr. Micheala Kleinert

Department of Physics

Willamette University, College of Liberal Arts
Salem, Oregon

2017

Presentations and Publications

Acknowledgments

Thanks to everyone! But really, thanks for reading my paper professors.



Abstract

My abstract goes here.

Table of Contents

Acknowledgments	iii
Abstract	iv
List of Tables	vii
List of Figures	viii
1 Introduction	1
2 Background	5
2.1 Quantum Theory of LGS	5
2.2 Magnetic Resonant Pulsing	8
2.3 Dye Lasers	11
2.4 Second Harmonic Generation	13
2.5 Diode Lasers and Acousto-Optic Modulators	15
3 Laser System	18
3.1 Duetto Laser	18
3.2 Second Harmonic Generation	18
3.3 Dye Laser Cavity	19
3.4 Diode Laser	19
4 Magnetic Field Housing	24
5 Absorption Spectroscopy	25
6 Conclusion	26

A Laser Guide Stars	27
B Adaptive Optics	32
Bibliography	35

List of Tables

List of Figures

1.1	Figure of a laser guide star being created at ESO's Very Large Telescope [ESO].	2
1.2	Cartoon of an atom with an angular momentum vector precessing around a magnetic field [Com].	3
2.1	Figure of the splitting of energy levels due to the fine, hyperfine, and Zeeman structure with principal quantum number n , angular momentum quantum number ℓ , total angular momentum quantum number j , total atomic angular momentum quantum number F , and magnetic quantum number m_F	8
2.2	Figure of optical pumping in which the excitation of the atom results in an angular momentum change of $\Delta m = +1$ but decay governed by $\Delta m = \pm 1, 0$ [CER].	9
2.3	Schematic of a dye laser with dye fluid in the dye cell being pumped by a laser input beam and lasing in a cavity consisting of a mirror and diffraction grating.	12
2.4	Depiction of second harmonic generation where an incoming photon, travelling through nonlinear crystal (yellow block), is converted into two photons, each with twice the frequency as the initial photon [SHG].	14
2.5	Figure showing the phase matching of the fundamental and second harmonic wave. In order to achieve maximum efficiency, $\Delta k \approx 0$	15
2.6	Schematic of an acousto-optic modulator. The dashed, red line is the laser beam coming from left to right and is diffracted by the AOM into a 1st- and 0- order beam [Tec].	16
3.1	Graph of the resistance of the thermistor as a function of its temperature, plotted with a line of best fit.	18
3.2	Spectrum of converted laser light before alignment of doubling crystal.	19

3.3	Conversion spectrum of laser light after alignment of doubling crystal.	19
3.4	Efficiency of the doubling crystal versus the resistance (and thus temperature) of the crystal. This, however, is simply an artifact the alignment of the crystal changing with temperature.	20
3.5	Graph of the fluctuations in resistance of the thermistor as temperature is varied.	20
3.6	Graph of the resistance of the thermistor versus temperature. . .	21
3.7	Graph of the temperature of the thermistor as it heats up.	21
3.8	Graph of the resistance of the thermistor as the crystal warms up. Line of best fit also plotted.	22
3.9	Graph of the temperature of the crystal plotted versus current through the transistor.	22
3.10	Figure of laser pulses from diode laser taken on an oscilloscope. . .	23
3.11	Figure of a zoomed in image of the diode pulse.	23
A.1	Schematic of a ray of light refracting according to Snell's Law as it passes from a medium of refractive index n_1 into a medium with higher refractive index n_2	27
A.2	Atmospheric distortion of a plane wave passing through Earth's atmosphere	28
A.3	Image of a sunset with atmospheric distortion disfiguring the spherical shape of the sun and creating sharp patterns on the edges [ST].	29
A.4	Schematic of sodium atoms residing in the mesosphere.	30
A.5	Image of a laser guide star being created at the Very Large Telescope [Uni].	30
B.1	Graph of the Airy disk function, describing an idealized point imaged through a spherically symmetric, aberration free optical system.	33

1 Introduction

In 1609, Galileo Galilei pointed a device of two lenses at the sky and saw for the first time tiny craters on the moon, small objects orbiting Jupiter, and even the phases of Venus [NAS03; Obs09]. With observations from this crude contraption, Galileo showed that Venus was orbiting the Sun. This evidence supported the theoretical model of a heliocentric universe, proposed in the sixteenth century by Nicolaus Copernicus and expounded upon by Johannes Kepler in the next century [JH01]. As time progressed, inquisitive minds began to wonder what else could be discovered with the power of magnification. Telescopes, as they would be coined, began a rapid period of advancement. Lenses were made larger in diameter in order to view fainter objects. Optical components were fabricated with less imperfection, allowing for better resolution. Curvature and indices of refraction of lenses were exploited, allowing for varying degrees of magnification. Achromatic, aspheric, and cylindrical lenses were created, ridding telescopes of significant aberrations. By the late twentieth century, telescopes were as optically perfect as they could be; no advancements in optics would allow them to see with greater magnification or increased resolution. However, there was a lingering problem: atmospheric distortion.

Atmospheric distortion is caused by the inhomogeneity of Earth's atmosphere. As light from astronomical bodies passes through the atmosphere, the varying levels of pressure, density, and temperature cause small distortions in the image of that object. In order to rid data of atmospheric distortions, astronomers image distance point sources, e.g. natural stars or laser guide stars, in order to calculate the distortion that the atmosphere is imposing on entering light. This distortion is then sent to a deformable mirror, which is able to form a conjugate wavefront that can effectively negate the atmospheric distortion. The image of the astronomical body is then reflected off this deformable mirror, and the resulting image is free of atmospheric distortion. This process is known as adaptive optics and is an image processing problem, not an optical component problem. (See Appendix B for more information on adaptive optics.)

In order to adaptive optics systems to work, there must be a bright enough

guide star in the sky; commonly however, artificial guide stars are created, known as laser guide stars. A laser guide star is created in the upper atmosphere by interacting laser light with sodium atoms that are deposited from meteors as they burn in Earth's atmosphere [Rob09]; an image of a laser guide star being created is shown in Figure 1.1. They are preferred over natural stars due to their ability to be spatially placed into the telescope's field of view, their brightness, and their well known spectral emission. Since the resolution of a telescope depends upon its adaptive optics system, and the adaptive optics system in turn depends upon the guide star, it is important to know how laser guide stars work and how they can be improved.



Figure 1.1: Figure of a laser guide star being created at ESO's Very Large Telescope [ESO].

One important property of laser guide stars is their brightness. The brightness can be increased by improving the intensity of the laser beam, increasing the size of the laser beam, or by using various optical techniques to increase the atom's probability of absorbing and emitting photons. Nevertheless, there remain "the three evils" of laser guide stars, each of which decreases brightness: Larmor precession, recoil, and transition saturation [RH10]. Larmor precession, shown in Figure 1.2, is the precession of the total atomic angular momentum vector about the geomagnetic field which decreases the benefits obtained from optical pumping. Recoil from spontaneous emission causes a redshift to occur, rendering the atom unable to absorb laser light [RH10]. Transition saturation is the depopulation of atoms from a state of higher angular momentum to a state of lower angular momentum, resulting in a different wavelength for absorbance [RH10]. We focus

on mitigating the effects Larmor precession has on the brightness of laser guide stars.

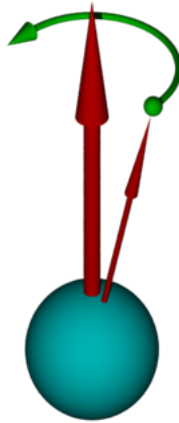




Figure 1.2: Cartoon of an atom with an angular momentum vector precessing around a magnetic field [Com].

In 2014, Kane et al. proposed a technique to improve laser guide stars, which he coined *magnetic resonant pulsing* (MRP). This technique proposes using a pulsed laser beam with a repetition rate equal to the Larmor frequency, the frequency of the atom's precession in the magnetic field; these frequencies are typically of a few hundred kilohertz [RR15]. MRP was computationally simulated by Rampy et al. [RR15] and Kane et al. [TJK14]. Their data show that lasers pulsed at the Larmor frequency of the atom in a magnetic field increase photon return as the laser beam nears perpendicular to the magnetic field. These data are consistent set forth by Kane et al. [TJK14].

In this thesis, we experimentally test MRP under controlled conditions. We investigate the construction of a magnetic resonant pulsed laser through both a short-cavity dye laser pumped by a frequency-doubled Nd:VO₄ and a diode laser chopped with an acousto-optic modulator (AOM). Rubidium was chosen because of its similarity to sodium, including a similar gyromagnetic ratio, magnetic moment, and Larmor frequency, in addition to both being alkali metals; it was also chosen over sodium in this experiment since the overall focus of this laboratory is concerned with rubidium. Absorption measurements are then taken of rubidium atoms confined in an absorption cell and surrounded by a magnetic field. The magnetic field is created using Helmholtz coils, adjustable in both their strength and orientation with respect to the incoming laser beam and capable of producing a magnetic field of about 10 G.

Since the Larmor precession of an atom depends on the strength of the magnetic field, we are able to change the frequency of rubidium's precession from

100 kHz to 300 kHz. Thus, we can bring the system into and out of magnetic resonant pulsing by adjusting the strength of the magnetic field while measuring the amount of light rubidium sorbs. By changing the orientation of the Helmholtz coils with respect to the laser beam, we are able to test the dependence of absorption upon the angle between the magnetic field and the laser beam. Together, se allow us to test magnetic resonant pulsing.

In Chapter 2, we outline the atomic and quantum theory that underpins laser guide stars, the details of magnetic resonant pulsing, dye lasers, second harmonic generation, and diode lasers and acousto-optic modulators. In Chapter 3, we detail the laser system capable of resonance with rubidium and pulsed at the Larmor frequency and provide data about this laser. Chapter 4 describes and provides data for the magnetic field configuration. In Chapter 5, we present the methods and results of the **absorption** measurements for the magnetic resonant pulsed system. Chapter 6 concludes this thesis and provides an outlook for future experiments.

2 Background

Laser guide stars (LGS)¹ are invaluable instruments in modern astronomy, allowing observations of extremely high resolution to be made even in unfavorable atmospheric conditions. An important quality of an LGS is its brightness, which affects the overall performance of the adaptive optics system and limits the resolution that the telescope can achieve. However, taking advantage of the atom's precession in a magnetic field, the brightness of LGS can be increased through magnetic resonant pulsing (MRP). In this chapter, we describe the quantum theory behind LGS, magnetic resonant pulsing, second harmonic generation, ultrafast dye lasers, as well as diode lasers and acousto-optic modulators (AOM).

2.1 Quantum Theory of LGS

As dictated by quantum mechanics, atoms have unique, quantized energy levels. In the simplest model, the electrons in the atom can be thought of as orbiting the nucleus; this model, proposed by Niels Bohr in the early nineteenth century, is known as the Bohr model. The electrons “orbit” in discrete radii of quantized energy, or shells, each of which is denoted by the principal quantum number n or $n = 1, 2, 3, \dots$. Each value of n can have an orbital quantum number of $0 \leq \ell < n$. Hence, for each shell of principal quantum number n , there exists a degeneracy of $n - 1$ given by the orbital angular momentum number ℓ .

Each electron shell refers to a certain energy of the atom, and electrons are free to transition between shells as long as energy is conserved during this transition.² As a pedagogical example, we can calculate the energy difference of an electron transitioning between shells for hydrogen using the famous Rydberg formula,

¹LGS will refer to both the plural and singular of the word, e.g. “LGS are frequently used in modern astronomy” and “LGS systems consist of many components.” Context should provide the correct form throughout reading this thesis.

²Other quantities, such as angular momentum, must also be conserved; these will be addressed shortly.

$$\Delta E = R \left(\frac{1}{n_f^2} - \frac{1}{n_i^2} \right), \quad (2.1)$$

where $R = 1.1 \times 10^7 \text{ m}^{-1}$ is the Rydberg constant, n_f is the final principal quantum number, and n_i is the initial principal quantum number. Empirically, we see that atoms emit photons when they decay from states of higher energy to those with lower energy. Knowing that the energy of a photon is

$$E = hf = \frac{hc}{\lambda}, \quad (2.2)$$

where h is Planck's constant, f is the frequency of the photon, c is the speed of light in a vacuum, and λ is the wavelength of the photon, we can calculate the wavelength of light a transition would emit using this and Equation 2.1,

$$\frac{1}{\lambda} = \frac{R}{hc} \left(\frac{1}{n_f^2} - \frac{1}{n_i^2} \right). \quad (2.3)$$

This process is also reversible, meaning we can actually excite an atom by sending a photon of wavelength equal to the energy difference of the corresponding transition; the frequency of light needed for this excitation is known as the resonant frequency. We can thus excite atoms by sending light of resonant frequency to the atom and in turn observe the light the atoms radiate upon decay. This is the foundation of LGS — laser light resonant with sodium is shone onto the sodium atoms in the atmosphere, the atoms absorb this light, and then emit light in random directions, creating a “globe” of light (See Appendix A for more discussion of laser guide stars).

The Bohr model, however, is not completely accurate. If we look carefully, we see that these energy levels actually consist of multiple, closely-spaced energy levels that are caused by the relativistic energy of the particles and the interaction between the electron's spin and its orbital angular momentum. Spin is a quantity that particles can possess, describing the particle's intrinsic angular momentum; it takes on integer or half integer values of the reduced Planck's constant. For example, electrons are spin- $\frac{1}{2}$ particles and thus have spin $= \pm \frac{\hbar}{2}$, while photons are spin-1 with $S = \pm \hbar$. Spin, being a value of the intrinsic angular momentum, can couple with the orbital angular momentum, causing an interaction that shifts and splits the energy levels; the relativistic kinetic energy simply shifts the energy. Collectively, these corrections are known as the *fine structure* [Kib09]. This splitting follows the formula

$$\vec{J} = \vec{L} + \vec{S}, \quad (2.4)$$

where \vec{L} is the orbital angular momentum and \vec{S} is the spin. The values that the splitting can thus take are $|j| = |l - s| + \dots + |l + s|$ in integer steps. Thus, for the $l = 0$ state of particle spin- $\frac{1}{2}$, $j = |0 - \frac{1}{2}| \dots |0 + \frac{1}{2}| = \frac{1}{2}$, indicating there only being an energy shift, and not split, for this state. However, for the $l = 1$ state, $j = |1 - \frac{1}{2}| \dots |1 + \frac{1}{2}| = |-\frac{1}{2}| \dots \frac{3}{2} = \frac{1}{2}, \frac{3}{2}$, indicating a two-fold split.

We can look even closer at the energy levels of atoms. We saw how \vec{J} interacted with the orbital angular momentum \vec{L} to cause an energy split, but \vec{J} can also interact with the spin of the nucleus, causing yet another, even smaller³ splitting of the energy levels. The hyperfine structure follows the formula

$$\vec{F} = \vec{J} + \vec{I}, \quad (2.5)$$

where \vec{I} is the nuclear spin. The splitting obeys $|j - i| \dots |j + i|$, causing degeneracy for all states with $j \neq 0$ and $I \neq 0$.

Finally, we can discuss the last relevant correction. If we consider the atom to be in a magnetic field, we get another splitting known as the Zeeman structure. The Zeeman structure results from a magnetic field interacting with \vec{F} , causing a precession of this vector about the axis of the magnetic field. The energy shift follows the equation

$$\Delta E = \mu_B m_j g_F B, \quad (2.6)$$

where μ_B is the Bohr magneton, m_j is the z-component of the total angular momentum, g_F is the Lande g -factor,⁴ and B is the magnetic field. The degeneracy is quantized by the values of the z-component of the orbital angular momentum, $m_l = -l \dots l$. As we will see in the next section, the energy splitting due to the Zeeman effect will be quite important. Since sodium, the basis of LGS systems, lives within the geomagnetic field, its energy is split due to the Zeeman effect. This turns out to have fascinating implications.

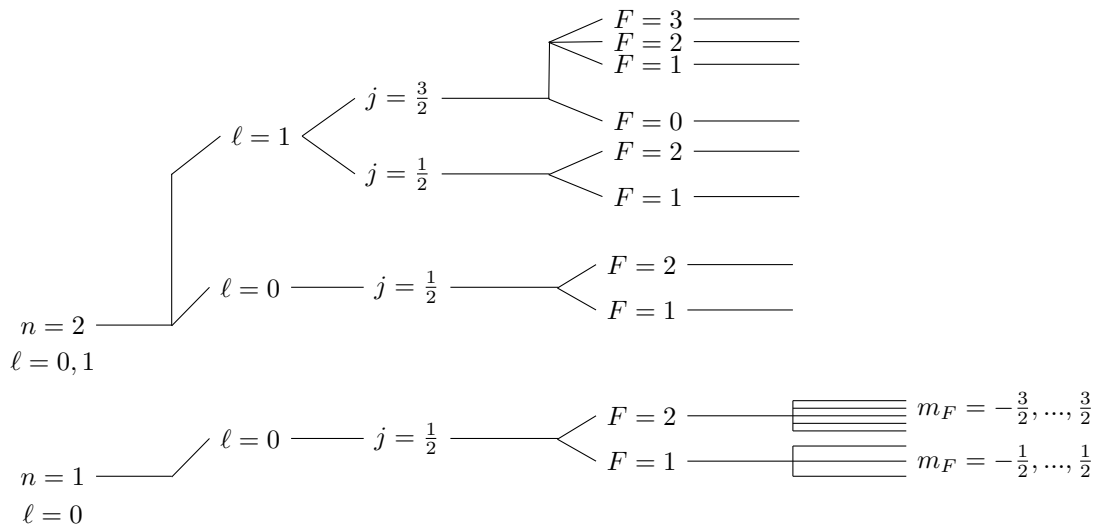
This is a lot to keep track of but can be shown schematically quite well. Figure 2.1 shows a schematic of the various structures. From left to right, the order of magnitude of the splitting gets smaller. As we move up vertically, we get varying levels of splitting depending on the quantum number involved.

³For hydrogen, these shifts are on the order of millionths of an eV [Fey65]; compared with the ionization energy of 13.6 eV, this is quite small.

⁴The Lande g -factor is a particular g -factor (dimensionless number describing the magnetic moment; see Section 2.2 for an introduction to the g -factor) that accounts for both the spin and orbital angular momentum of the particle. It is described mathematically as

$$g_F = g_J \frac{F(F+1) - I(I+1) + J(J+1)}{2F(F+1)} + g_I \frac{F(F+1) + I(I+1) - J(J+1)}{2F(F+1)} \quad (2.7)$$

where $g_{J,I}$ are the Lande g -factors for the those particular quantum values, and F, J, I are the



Bohr Fine Hyperfine Zeeman

Figure 2.1: Figure of the splitting of energy levels due to the fine, hyperfine, and Zeeman structure with principal quantum number n , angular momentum quantum number ℓ , total angular momentum quantum number j , total atomic angular momentum quantum number F , and magnetic quantum number m_F .

These transitions are the basis for the absorption and emission of light by atoms. For sodium, the ground state is split into two levels, creating two distinct transitions, from $3P_{3/2}$ to $3S_{1/2}$ and $3P_{1/2}$ to $3S_{1/2}$ [Kib09], where s,p refer to angular momentum values of $\ell = 0, 1$ respectively, the number in front refers to the principal quantum number n , and the subscript refers to the total angular momentum quantum number; these transitions have respective wavelengths 894.99 nm and 589.59 nm [Kib09]. For rubidium 87, the transition between the $5P_{3/2}$ to $5S_{1/2}$ has a wavelength of 780.24 nm [Ste01]. This rubidium transition, well at the $3P_{3/2}$ to $3S_{1/2}$, is known as the D_2 transition. The D_2 line of sodium is the main transition used to create laser guide stars in the atmosphere.

2.2 Magnetic Resonant Pulsing

One technique that is often used in LGS to increase brightness is the use of circularly polarized laser light. Photons can carry spin angular momentum (SAM), and due to conservation of angular momentum, this momentum is imparted to

quantum values discussed earlier.

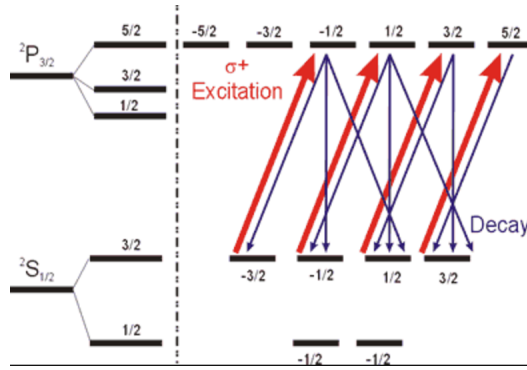


Figure 2.2: **Figure** of optical pumping in which the excitation of the atom results in an angular momentum change of $\Delta m = +1$ but decay governed by $\Delta m = \pm 1, 0$ [CER].

the atom during absorption. When an atom absorbs a photon with SAM of $S_z = \pm\hbar$, the angular momentum of the atom must increase by the same amount, $\Delta m_J = \pm\hbar$. However, when the atom emits a photon, it can decay to any state satisfying $\Delta m_J = \pm\hbar, 0$. However, the probability of decreasing angular momentum upon emission is significantly lower than a change of $\Delta m = 0, 1$. Hence, atoms tend to move towards states of higher angular momentum and eventually end up in a cyclical transition between the states of highest angular momentum. This process, shown in Figure 2.2, is known as *optical pumping* [TJK14]. By pumping all atoms into this two-level transition, we ensure that the atoms can only have one decay path with 100% probability, increasing photon emission and absorption by a factor of 3 [Kib09].

However, when exposed to an external magnetic field, the \vec{F} vector will tend to precess about the magnetic field; this is known as *Larmor precession*. Classically, this precession can be thought of as due to the torque a magnetic field exerts on the atom,

$$\vec{\tau} = \vec{\mu} \times \vec{B}, \quad (2.8)$$

where $\vec{\mu}$ is the magnetic moment of the atom and \vec{B} is the external magnetic field. This equation can be rewritten by noting that the **magnetic moment** is the product of the gyromagnetic ratio and angular momentum of the atom,

$$\vec{\mu} = \gamma \vec{J}, \quad (2.9)$$

where \vec{J} is the atom's combined angular momentum and $\gamma = \frac{eg}{2m}$ is the gyro-

magnetic ratio with e being the charge of an electron, g being the g-factor,⁵ and m being the mass of the atom. The **torque** can then be written as

$$\vec{\tau} = \gamma \vec{J} \times \vec{B}. \quad (2.10)$$

The angular frequency of this precession, known as the *Larmor frequency*, can be found by solving $\vec{\tau} = \frac{d\vec{L}}{dt}$, giving

$$\omega = \gamma B. \quad (2.11)$$

From the Larmor frequency, we can compute the energy shift due to the magnetic field. This shift is

$$\Delta E = \hbar \omega. \quad (2.12)$$

Larmor precession can actually degrade the benefits obtained by optical pumping. Optical pumping relies on redistributing the angular momentum of the atom, but for a magnetic field not aligned with the direction of the laser beam, this redistribution **now** does not distribute angular momentum perfectly since the magnetic field reorients \vec{F} . Typically, the magnetic field reorients the atom much faster than the benefits of optical pumping can be obtained [TJK14]. Thus, the increase in absorption and emission is greatly reduced for atoms exposed to a magnetic field.

However, if we substitute the energy shift from the Zeeman effect, given by Equation 2.6, into Equation 2.12, we can find the frequency of the atom's **precession**

$$f_Z = \frac{1}{h} g_F n_j g_F B. \quad (2.13)$$

Knowing this frequency is **incredibly valuable**. If instead of pumping the atoms continuously with light (using a CW laser), we can optically pump the atoms with light that is pulsed at a repetition rate equal to this frequency. This allows the light to only “talk” to the atoms at one point in the precession cycle as if the particle **was** not precessing at all. The benefits of optical pumping can be reestablished with this technique, since a cycling transition can be reached without the combined angular momentum \vec{F} changing with time. This technique is **magnetic resonant pulsing**⁶

⁵The g-factor, or g-value, is a dimensionless value that arises from a quantum treatment of the atom; it essentially accounts for the quantization of angular momentum of the nucleus.

⁶The idea of magnetic resonant pulsing is analogous to pushing a **kid** on a swing. If you apply a constant force the whole time, your **kid won't** establish a nice oscillation. However, if you give a good push at one point each oscillation, your kid will soon be swinging quite high on the swing set.

2.3 Dye Lasers

Dye lasers were **some** of the first lasers to be used as laser guide stars [Pri91]. This is due to a variety of factors: their wavelength can be precisely tuned over a broad spectral range, they are relatively inexpensive and easy to use, and they are fairly robust. In the modern age, many telescopes have opted for solid state lasers because of their efficiency and reliability [PW06]. Nevertheless, dye lasers will be explained in this section not only because of their pedagogical importance, but because they are **one laser system** we investigate for magnetic resonant pulsing.

Laser is an acronym for *light amplification by stimulated emission of radiation*. In general, a laser consists of three parts: a pump, a medium, and a cavity. The pump provides enough energy to move atoms in the medium into the excited state. The atoms then decay back into their ground state, releasing a photon in a random **direction, known** as spontaneous emission. However, a spontaneously emitted photon travelling through the medium can interact with an excited atom, causing what is known as stimulated emission; this causes the excited atom to decay to its ground state, releasing a photon with the same direction, frequency, phase, and polarization as the initial photon. A cavity can be created around the medium, typically by placing mirrors on either side of the medium, causing the photons to travel back and forth in the medium, stimulating the emission of more and more photons. These photons will continue to build, creating a powerful source of monochromatic, coherent light. One of the cavity mirrors is commonly made partially transmissive, allowing only a certain percentage of photons to pass through. These photons passing through the partially transmissive mirror form the usable laser beam. **This is the foundation of a laser.**

A dye laser works in exactly the same way. Its medium is a fluorescent dye in a solvent such as **alcohol**. Typically, the pump is another laser with a frequency of light corresponding to the absorption wavelength of the dye molecules. The cavity can vary in design, but normally consists of a mirror at one end and a diffraction grating at the other [JES97]. The diffraction grating spreads out the various wavelengths of **light, allows** a specific wavelength to be **reflected back** into the cavity through alignment of the **grating; this results** in a range of accessible wavelengths the system can lase at (tunability), typically on the order of a few tens of **nanoseconds** [JES97].

The big advantage of dye lasers is their incredible tunability over a broad **spectral range**. This is a consequence of the lasing medium; **being relatively large chain molecules, the fluorescent dye, once excited by the pump, relaxes in energy due to the many vibrational and rotational states it can reside in.** These relaxations result in photons of varying wavelength being emitted spontaneously. In order to access and select these different wavelengths, the diffraction grating is used to split apart the various wavelengths, sending the desired lasing wavelength back into the medium.

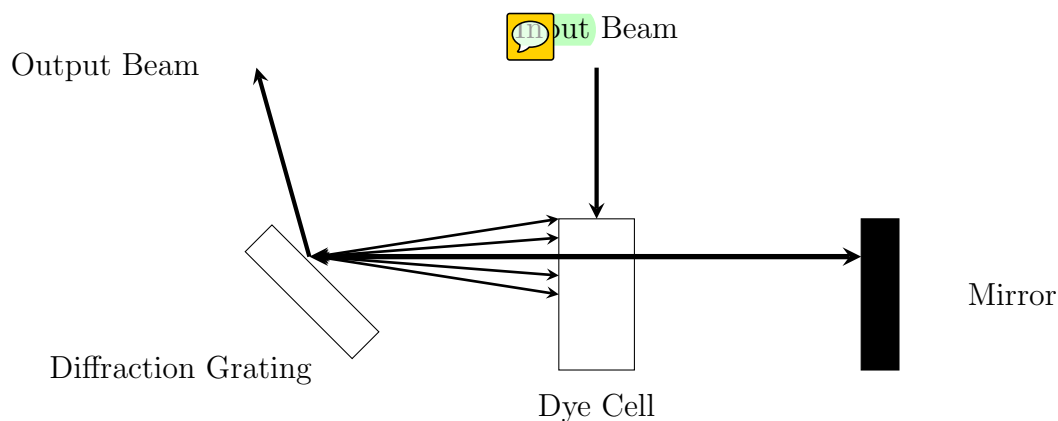


Figure 2.3: Schematic of a dye laser with dye fluid in the dye cell being pumped by a laser input beam and lasing in a cavity consisting of a mirror and diffraction grating.

An ultrashort pulsed dye laser, with pulse widths on the order of picoseconds and repetition rates of hundreds of kilohertz, is significantly more difficult to construct than a CW or long pulse dye laser. In order to create a significant amount of stimulated emission, photons must have enough time to travel back and forth through the cavity a few times⁷ to induce the stimulated emission of more photons from molecules in an excited state. However, for ultrashort pulses, there is only a few picoseconds of time for the light to interact with the molecules. Once the pulse has excited the molecules, there is then a certain **length of time** the atoms will stay excited, known as the lifetime of the dye; the dye we will be using has a lifetime of a few nanoseconds [KS77]. In this time, the photons need to be able to pass back and forth through the cavity ten times. The length of the cavity must then be on the order of

$$\begin{aligned}
 L &= \frac{1}{10} c \tau \\
 &= \frac{1}{10} (3 \times 10^8 \text{ m s}^{-1}) (4 \times 10^{-9} \text{ s}) \\
 &\approx 0.029 \text{ m},
 \end{aligned} \tag{2.14}$$

where L is the total length of the lasing cavity, c is the speed of light, and τ is lifetime of the dye. Experimentally, 3 cm is a pretty tight fit for a **lab**-built cavity. Furthermore, because of the short interaction time between the pulse and the molecules, it is possible not enough molecules are being excited per laser pulse. Thus, constructing and aligning this laser will prove difficult.

⁷Technically, only one pass through the cavity is sufficient, but increasing to around 10 passes allows for a significant narrowing of the linewidth.

2.4 Second Harmonic Generation

A significant part of a dye laser is the pump source for exciting the medium. A common way to pump a dye laser is with another laser of wavelength equal to that of the absorption wavelength of the dye. The dye we will use has an absorption wavelength in the green, visible range of the spectrum. However, the laser we have, capable of a repetition rate equal to the Larmor frequency, lases in the infrared at $\lambda = 1064 \text{ nm}$. Thus, we need to convert 1064 nm light into something closer to green light. This can be done using a frequency doubling crystal, which essentially converts one photon of 1064 nm into two photons of 532 nm. This is known as second harmonic generation and is outlined in this section.

The electric field of a wave can be described by

$$E_i = \varepsilon_i e^{-i\omega t}, \quad (2.15)$$

where ε_i is the amplitude of the field at the given position, ω is the frequency, and t is a time dependence [dD06]. For a linear crystal, the polarization can be described by a linear function

$$\vec{P} = \epsilon_0 \chi^{(1)} \vec{E}, \quad (2.16)$$

where ϵ_0 is the permittivity of free space, $\chi^{(1)}$ is the linear electric susceptibility,⁸ and \vec{E} is the induced electric field. The polarization is thus the electric field multiplied by a constant.

However, things behave much differently when we introduce a nonlinear crystal. This type of crystal has a nonlinear polarization function and, using a Taylor expansion, we can write this polarization as

$$\vec{P} = \epsilon_0 \left(\chi_{ik}^{(1)} E_i + \chi_{ijk}^{(2)} E_i E_j + \chi_{ijkl}^{(3)} E_i E_j E_l + \dots \right), \quad (2.17)$$

where each $\chi^{(n)}$ represents the tensor of the n^{th} susceptibility and the notation $\chi_{ik} E_i$ corresponds to an Einstein summation.⁹ If we now substitute in the electric field from Equation 2.15, we see that we will get terms of order E^2 . If we look specifically at the polarization for these second order terms, we find that the polarization is

$$P_k = \epsilon_0 \left(\varepsilon_i \varepsilon_j e^{-2i\omega t} + \varepsilon_i^* \varepsilon_j^* e^{2i\omega t} + \varepsilon_i^* \varepsilon_j + \varepsilon_i \varepsilon_j^* \right), \quad (2.18)$$

⁸The linear electric susceptibility is a constant that relates polarization inside a medium to induced electric field; it is given by $\chi = \epsilon_r$ where ϵ_r is the dielectric constant. Thus, in a vacuum where $\epsilon_r = 1$, we can see $\chi = 0$.

⁹Einstein notation is a shorthand way of writing summations. For any repeated indices, we compute a summation over that index; for example, $\chi_{ik} E_i = \sum_{i=1} \chi_{ik} E_i$.

where the superscript $*$ denotes complex conjugate and $\mathbf{k} = (x, y, z)$. Thus, we find terms of $e^{2i\omega t}$, implying that not only do we have the linear field with frequency ω , but we have picked up a field with frequency 2ω [dD06]. In the crystals we will be using, the second-order term will dominate when the laser intensity is high, implying a majority of light is frequency doubled by the nonlinear term and a negligible amount of light passes through without being doubled.

This is second harmonic generation, or frequency doubling. It is a process that occurs in nonlinear crystal where a photon of frequency f_1 is converted into two photons each of frequency f_2 with $f_1 = f_2$. Since the energy of a photon is linearly proportional to its frequency, this makes intuitive sense from a conservation of energy perspective. A depiction of this is shown in Figure 2.4, where the initial light is known as the fundamental wave and frequency doubled light is known as the second harmonic wave.

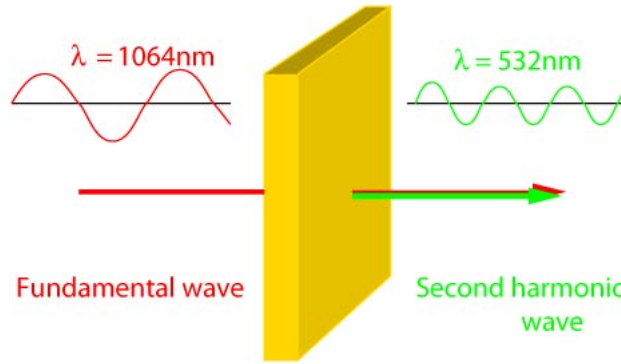


Figure 2.4: Depiction of second harmonic generation where an incoming photon, travelling through nonlinear crystal (yellow block), is converted into two photons, each with twice the frequency as the initial photon [SHG].

In order to achieve maximum efficiency during a frequency doubling conversion, we need the phase difference between the fundamental and second harmonic to be approximately zero; this ensures no destructive interference will occur. The necessary condition is shown in Figure 2.5, with the wave-vector k of the fundamental and second harmonic wave shown; the wave-vector is a vector of magnitude equal to the wavenumber (inverse wavelength) of the wave and direction equal to the propagation direction.

Mathematically, we can define the phase difference Δk as the sum of the fundamental wave-vector plus twice the second harmonic wave-vector. This relation is

$$\Delta k = k_1 + 2k_2 \quad (2.19)$$

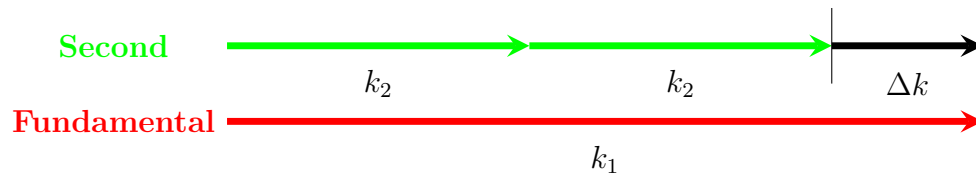


Figure 2.5: Figure showing the phase matching of the fundamental and second harmonic wave. In order to achieve maximum efficiency, $\Delta k \approx 0$.

where k_1 is the phase of the fundamental wave, and k_2 is the phase of the second harmonic. Having a phase difference of $\Delta k = 0$ ensures that no destructive interference between the waves will occur, resulting in maximum output power.

2.5 Diode Lasers and Acousto-Optic Modulators

This section was added after the first draft with not much time to research and edit

In addition to investigating the use of dye lasers as a MRP laser system, we also investigate the use of a diode laser, pulsed by chopping the beam with an acousto-optic modulator (AOM), as a MRP laser system. The diode laser system will turn out to be much simpler and just as effective as the dye laser system.

A diode laser is a semiconductor device which makes use of a P-N junction to produce stimulated emission. This P-N junction is two semiconductors placed side by side, one being P-doped and the other being N-doped; P-doping places atoms with valence shells not completely full in the semiconductor while N-doping places atoms with valence shells containing only a few electrons. If a voltage is placed across this junction, electrons from the N-doped semiconductor will be pushed towards the P-doped semiconductor. This situation then allows for the electrons to decay into the “holes” provided by the P-donors, emitting a photon on decay. This can then be turned into a laser by creating a cavity around this configuration.

The wavelength of light emitted from laser diodes is dependent upon the material of the semiconductor; many different diode lasers are available with various wavelengths, including 780 nm for rubidium absorption. Typically, laser diodes have a bandwidth of a few nanometers, but a specific wavelength of light can be selected from this bandwidth with a method similar to that of the dye laser. Using a diffraction grating, light from the diode laser can be spread out and reflected back into the laser diode. The particular wavelength reflected back into the diode will stimulate the emission of photons of similar wavelength, thereby narrowing the bandwidth.

Diode lasers are, however, continuous wave lasers. In order to make a pulsed diode laser, we use an acousto-optic modulator. This is a device that makes use of the propagation of sound waves through a crystal to diffract light. A schematic of an AOM is shown in the Figure 2.6. A crystal is attached to a piezo-electric transducer (T) which can be driven by an electric signal. If a periodic signal is given to the PET, it will oscillate back and forth in a periodic manner. This sends compressions along the crystal, which act similar to sound waves travelling through a solid. It can quantize these oscillations and think of them as particles, known as phonons. As light enters the crystal, perpendicular to the propagation direction of the sound wave, the photons will come into contact with the phonons, and by conservation of momentum, be deflected. This creates a “diffracted” beam of first order.

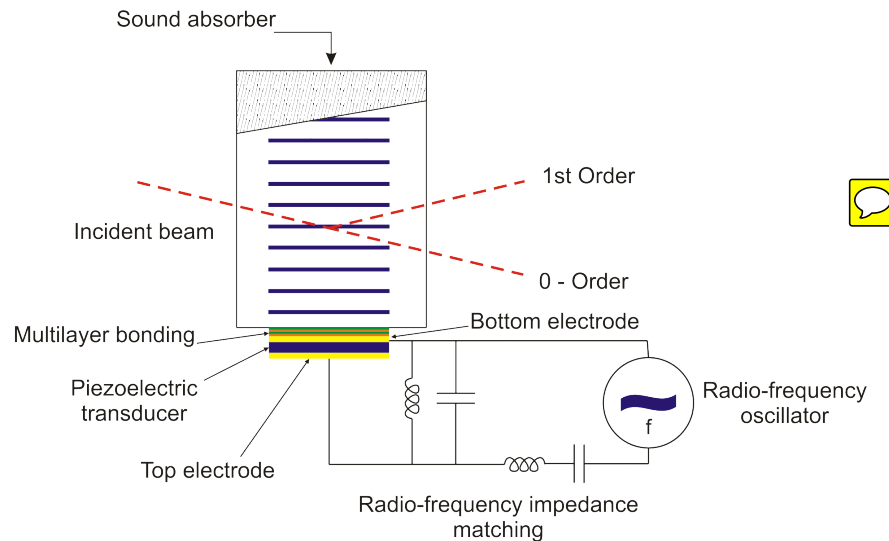


Figure 2.6: Schematic of an acousto-optic modulator. The dashed, red line is the laser beam coming from left to right and is diffracted by the AOM into a 1st- and 0- order beam [Tec].

If we take the 1st-order beam to be our laser beam, we can create a pulsed laser simply by turning on and off the PET; when the PET is turned on, it will diffract the incoming beam, creating a pulse of light, and when it is turned off, the incoming beam will no longer be diffracted and the pulse will be cut off. Thus, the length of time the PET is turned on for will determine the pulse width of our laser, and the frequency at which we turn the PET on and off will determine the repetition rate of the laser.

In this chapter, we have described the necessary theory that underpins this thesis. We have explained the quantum theory of laser guide stars, magnetic resonant pulsing, dye lasers, second harmonic generation, and diode lasers and

acousto-optic modulators. In the next chapter, we will discuss our experimental methods and results to test the effects of magnetic resonant pulsing.

3 Laser System



3.1 Duetto Laser

rep rate, pulse length, power, energy, about

3.2 Second Harmonic Generation

crystal, properties, data about resistance and conversion eff.

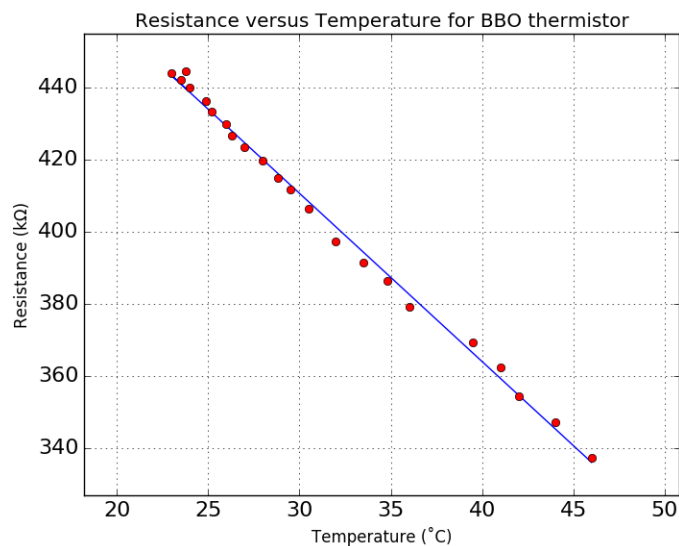


Figure 3.1: Graph of the resistance of the thermistor as a function of its temperature, plotted with a line of best fit.

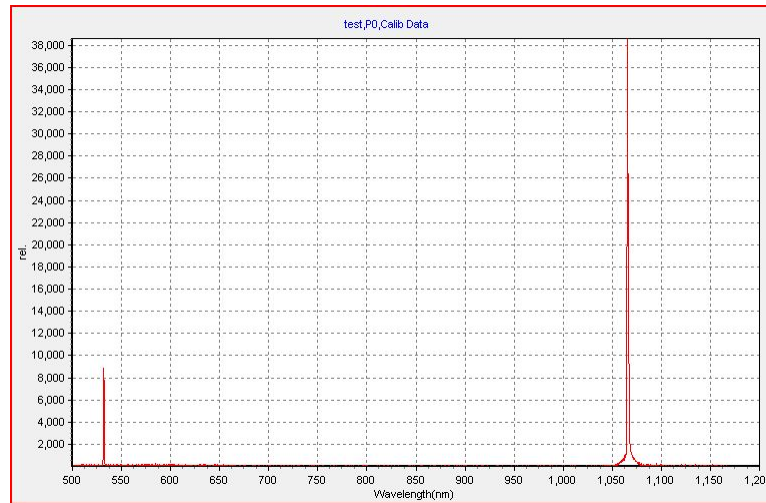


Figure 3.2: Spectrum of converted laser light before alignment of doubling crystal.

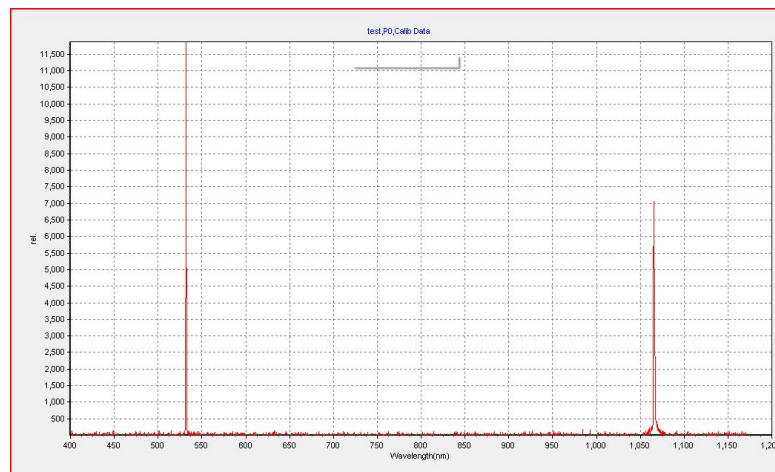


Figure 3.3: Conversion spectrum of laser light after alignment of doubling crystal.

3.3 Dye Laser Cavity

Critical length, methods of alignment, Wavelength and tunability, spectra

3.4 Diode Laser

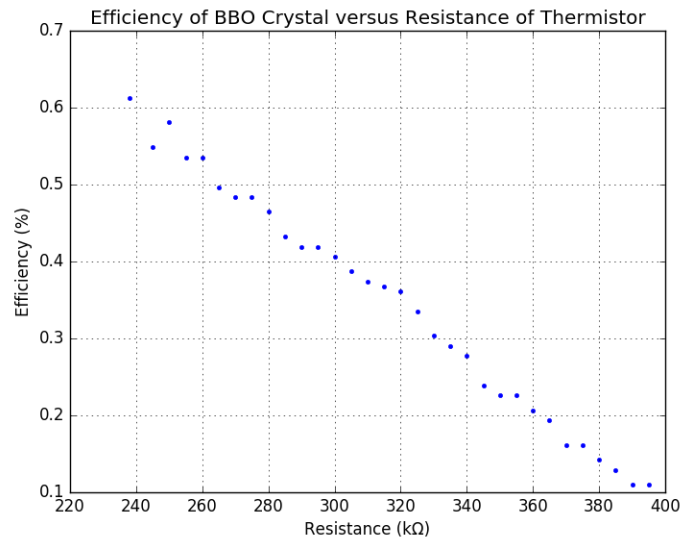


Figure 3.4: Efficiency of the doubling crystal versus the resistance (and thus temperature) of the crystal. This, however, is simply an artifact the alignment of the crystal changing with temperature.

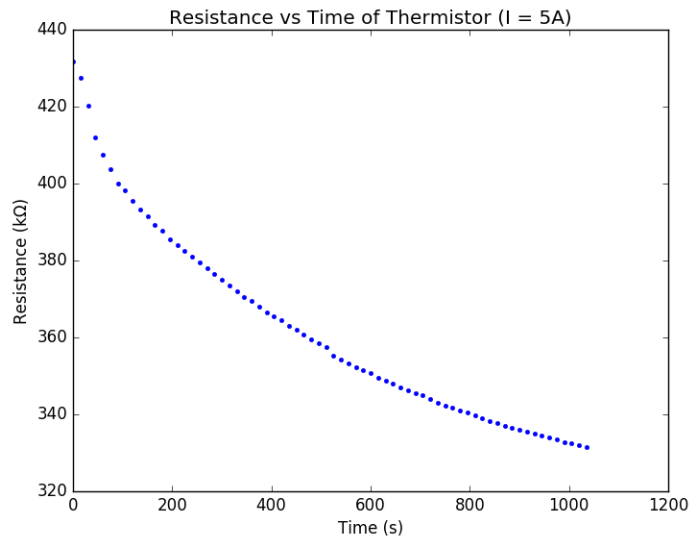


Figure 3.5: Graph of the fluctuations in resistance of the thermistor as temperature is varied.

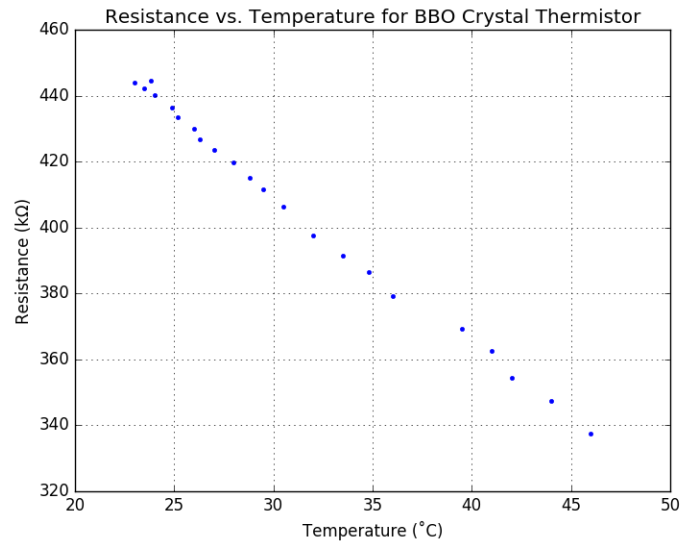


Figure 3.6: Graph of the resistance of the thermistor versus temperature.

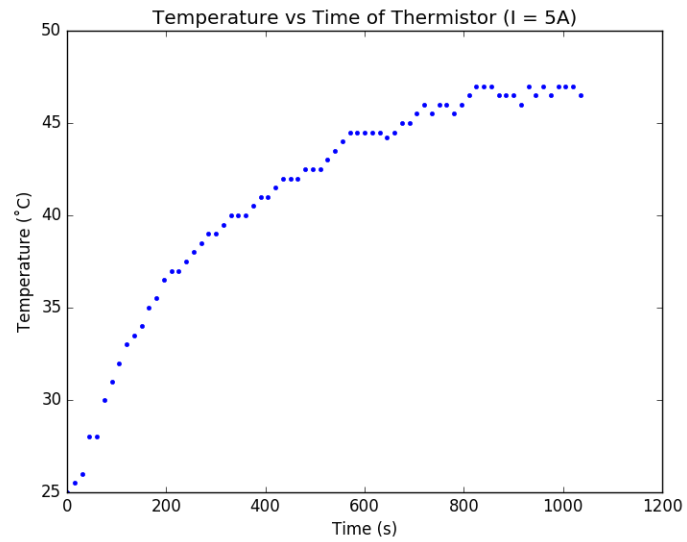


Figure 3.7: Graph of the temperature of the thermistor as it heats up.

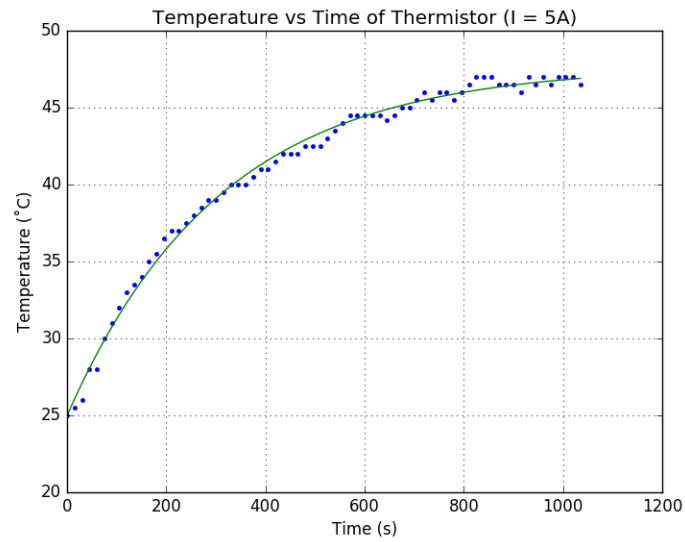


Figure 3.8: Graph of the resistance of the thermistor as the crystal warms up. Line of best fit also plotted.

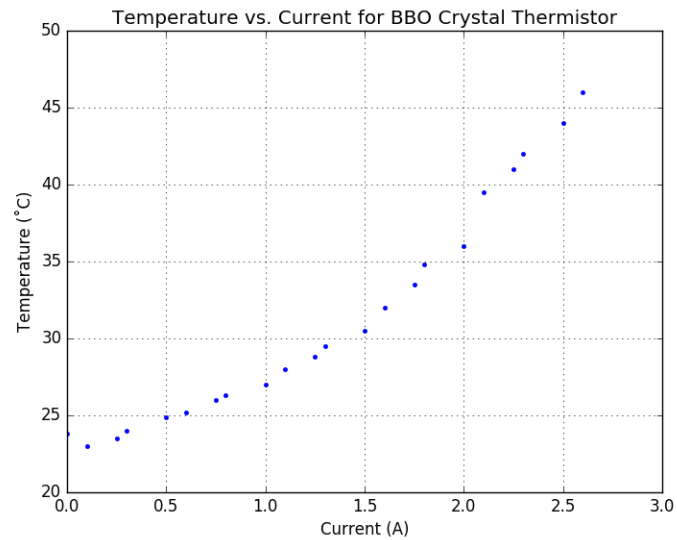


Figure 3.9: Graph of the temperature of the crystal plotted versus current through the transistor.

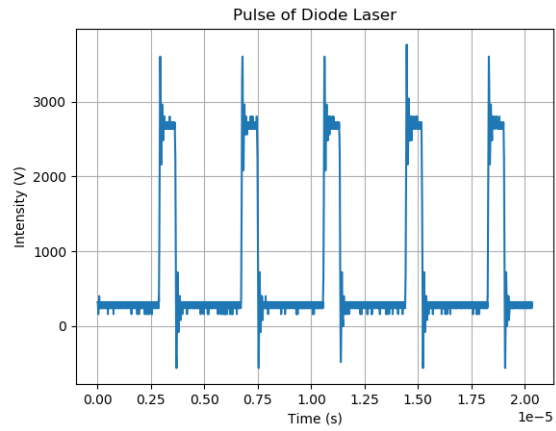


Figure 3.10: Figure of laser pulses from diode laser taken on an oscilloscope.

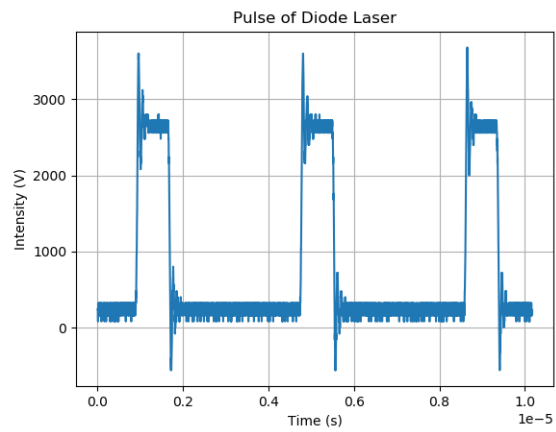


Figure 3.11: Figure of a zoomed in image of the diode pulse.

4 Magnetic Field Housing

Calculate gyromagnetic ratio, larmor frequency, magnetic field required, current required, geometry, testing, magnetic field data, homogeneity stability

5 Absorption Spectroscopy


absorption spectroscopy of rubidium with pulsed dye laser. Show difference in absorption (or no difference) when repetition rate is equal to that of the larmor precession (determined by magnetic field)

6 Conclusion

Conclude everything, did it work, did it not work, where should people go next, what is the significance



A Laser Guide Stars

Telescopes observing distant astronomical objects face a significant challenge known as atmospheric distortion. Light coming from these astronomical objects travels in a straight line with little obstruction in the near vacuum of space. However, as a ray of light travels from free space into the atmosphere of Earth, it is affected by the many gaseous particles that make up the atmosphere. The effect is a bending of the light s, known as *refraction*, that can be described mathematically by Snell's Law,

$$n_1 \sin \theta_1 = n_2 \sin \theta_2, \quad (\text{A.1})$$

where n_1 is the index of refraction of the first medium, n_2 is the refractive index of the second medium, and θ_1 and θ_2 are the angles that the ray makes with the normal to the interface between the media; a schematic of this is shown in Figure A.1.

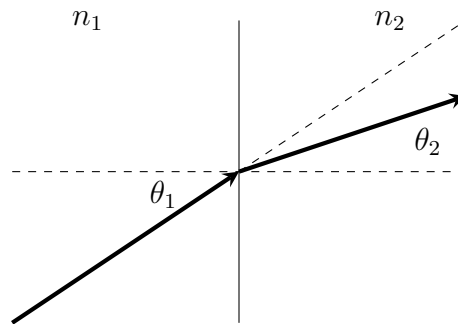


Figure A.1: Schematic of a ray of light refracting according to Snell's Law as it passes from a medium of refractive index n_1 into a medium with higher refractive index n_2 .

In general, the many light rays that make up the observed object will be refracted uniformly, causing the object to be perceived in a location that is different

from its true position. While that alone is not a problem, if we look closer, we find that the atmosphere does not refract all light rays in the same manner, but small variations in pressure, temperature, and density cause a change in the index of refraction, resulting in light rays that are close together to be refracted in slightly different ways; this is known as *atmospheric distortion*. A schematic is shown in Figure A.2, with plane waves being distorted as they pass through an atmosphere.

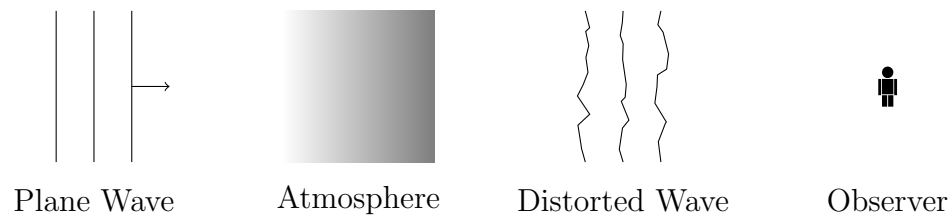


Figure A.2: Atmospheric distortion of a plane wave passing through Earth's atmosphere

The idea of atmospheric distortion will be familiar to those who have seen the sunset on the horizon. As the sun nears the horizon, the light is bent strongly through the atmosphere, resulting in much more distortion than when high in the sky. This results in a disfiguring of its **spherical** shape and a **sharpening** around the edges. An example of this is shown in Figure A.3.

In order for telescopes to improve resolution, astronomers need to find a way to rid their systems of this atmospheric distortion. One way to do this is to place the telescope outside of Earth's atmosphere where it would be unaffected by atmospheric distortion. This was done with amazing success in 1990 with the low-orbiting, powerful Hubble telescope [Oko]. However, it is not only extremely costly to put telescopes into orbit, but also impractical as they cannot be easily maintained or serviced.

Thus, a different solution was **proposed**. If astronomers could model how the light was distorted as it passed through the atmosphere, they could subtract those distortions from their images and obtain higher resolution data. In order to measure the amount of distortion, telescopes can observe a point source in the sky, such as a distant star, and observe its image. This image is then compared with the image of an ideal point source, and the difference between these two images gives the amount of distortion. Once the distortion is known, it is sent to a deformable mirror; this deformable mirror is made of many smaller mirrors, each able to move independently from the others. The deformable mirror can then create a wavefront conjugate to the distortion calculated. By reflecting the image of astronomical object off this mirror, the distortion is removed from the image. This process is known as *adaptive optics*, and more information is given in Appendix B.

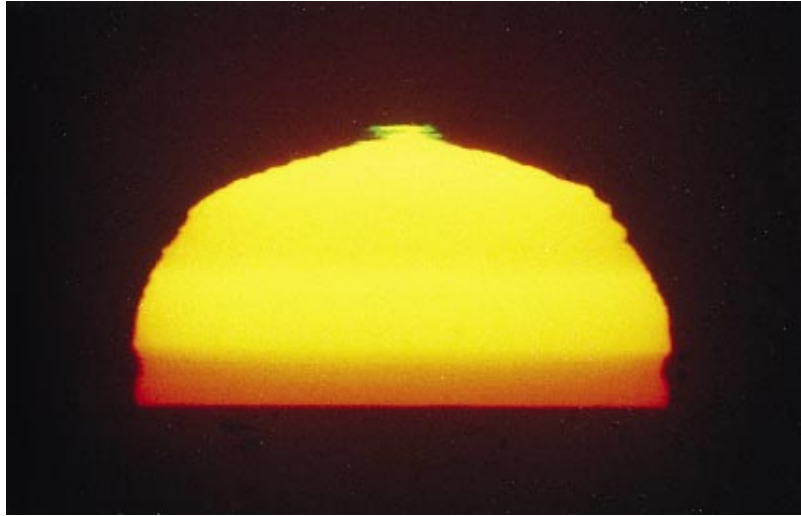


Figure A.3: Image of a sunset with atmospheric distortion disfiguring the spherical shape of the sun and creating sharp patterns on the edges [ST].

However, there are not always stars bright enough in the telescope's field of view that can be used as the point source, or guide star [PW06]. In order to skirt this problem, artificial stars were constructed, known as *laser guide stars*. A laser guide star is created by sending laser light into the atmosphere, where it interacts with a layer of sodium atoms. These sodium atoms reside approximately 60 km from Earth in a 10 km thick layer of the atmosphere known as the mesosphere [Kib09]; a figure of this region within the layers of Earth's atmosphere is shown in Figure A.4. These atoms are deposited from meteorites as they burn up in Earth's atmosphere, leaving behind their composite particles, a significant portion being sodium metal [Kib09]. The density of this sodium layer varies throughout a given day and throughout the year, but typically is near 5×10^{13} atoms/m³ [Kib09]. Using a laser with a wavelength resonant with sodium, the atoms will absorb and emit this laser light, creating a glowing sphere in the upper atmosphere, as described in Chapter 2. This sphere of light is then used as the guide star.

In general, most large-scale, ground-based telescopes now have powerful lasers with wavelengths precisely tuned to be resonant with sodium. While these telescopes are making observations, the lasers are shone into the sky to create the LGS; an image of a LGS being created is shown in Figure A.5. The LGS is observed and atmospheric distortions are calculated and subtracted from the image in real time.

One major concern for LGS systems is their brightness in the sky [PW06]. It is important for the star to be bright enough that the telescope system is able to pick up enough light for measurement of the distortion. The shape of the LGS is also important, as it must be as near to circular as possible in order for an

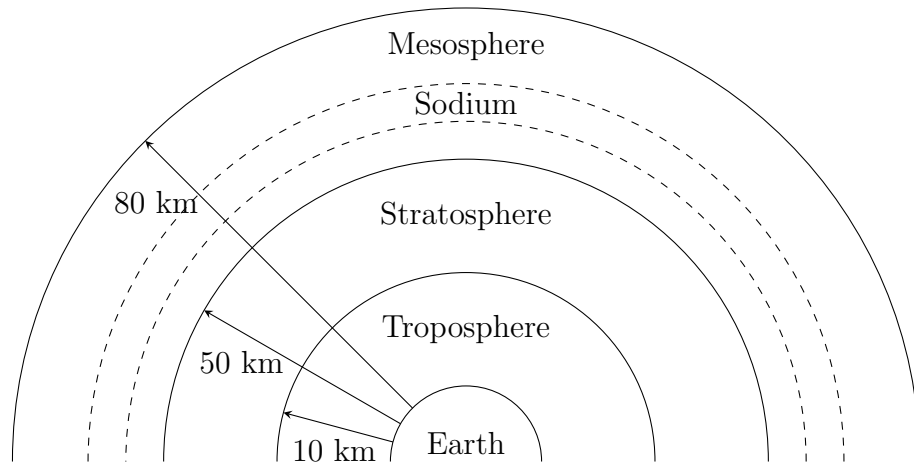


Figure A.4: Schematic of sodium atoms residing in the mesosphere.

accurate measurement of the distortion to be made. The shape of the LGS is mostly due to the profile of the laser beam [RH10], and will not be discussed here.

In order to create a brighter laser guide star, a few methods are utilized. One method is to increase the intensity, the power per unit area, of the laser. This will allow for more atoms to absorb and emit light, thereby creating a brighter star. Another method is to increase the diameter of the laser beam, which will



Figure A.5: Image of a laser guide star being created at the Very Large Telescope [Uni].

allow for a greater area of sodium atoms to be reached by the light. A more sophisticated method, optical pumping (discussed in Chapter 2), makes use of circularly polarized light to move the atom into a cycling transition. The method explored in this thesis takes advantage of the geomagnetic field, the Zeeman effect, and a pulsed laser to increase the brightness of LGS.



B Adaptive Optics

The process of measuring the atmospheric distortion in order to enhance astronomical imaging, known as *adaptive optics*, turns out to be quite tricky. Here, we present an introduction to the methods used during this process.

In general, telescopes observe the LGS and the astronomical object simultaneously. The image of the LGS is then compared to an ideal point source imaged through the telescope, and the distortion is calculated by comparing the two. A deformable mirror, composed of many smaller errors each of which can be moved independently of the others, is then used to create the opposite of the calculated distortion. The image of the astronomical object is then reflected off this mirror, thereby ridding the image of distortion.

In order to calculate the atmospheric distortion, astronomers make use of the well defined way in which point sources are imaged through optical systems. When an idealized point is imaged through an optical system, it has a certain energy distribution in image space, known as the point spread function. For an optical system with spherical symmetry and no aberration, the point spread function can be described mathematically along one coordinate as

$$P(x) = \frac{J_1(x)}{x}, \quad (\text{B.1})$$

where $J_1(x)$ is the Bessel function of first kind. This function is known as the *Airy disk*, and is shown in Figure B.1; it is an idealized description of a **point** imaged through a perfect optical system.

It turns out that stars are very close to being idealized point sources and can thus be used as this idealized point source. Since the light from these stars is passing through Earth's atmosphere, it will be distorted, and these distortions will show up in the point spread function, is deviating from the Airy Disk described by Equation B.1.

Astronomers then use a combination of Fourier mathematics and an optimization algorithm to calculate the distortion; this method follows that outlined by Gonsalves [Gon82]. **This is done** by first calculating optical transfer function

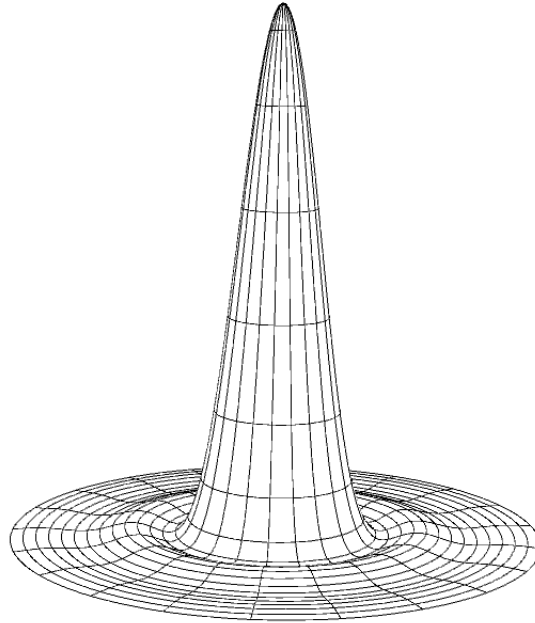


Figure B.1: Graph of the Airy disk function, describing an idealized point imaged through a spherically symmetric, aberration free optical system.

$$H(\omega) = A(\omega)e^{i\theta} \quad (\text{B.2})$$

where $A(\omega)$ is the aperture function¹ of the system and $\theta(\omega)$ is the phase of the incoming light. The phase of the light can be described as a summation:

$$\theta(\omega) = \sum_{k=0}^{\infty} c_k \phi(\omega) \quad (\text{B.3})$$

where $\{\phi(\omega)\}$ is a set of polynomials² and c_k is a coefficient that quantifies how much of each polynomial is present in the distortion. Taking the inverse Fourier transform and then the modulus squared, we can calculate the point spread function of this system.

¹The aperture function is normally a function describing where light can and cannot pass through. For a circular aperture, it would consist of a solid circle where light can pass through and nothing around the circle; it essentially acts like the computational version of a camera aperture.

²The idea of using a set of polynomials to describe the phase is similar to the idea of using sinusoidal functions in Fourier analysis to deconstruct a signal.

$$P(x) = \left| \text{ifft}[H(\omega)] \right|^2 \quad (\text{B.4})$$

where ifft denotes the inverse Fourier transform of the argument. This method allows us to mathematically create a point spread function simply by estimating the phase of the light with a set of polynomials.




Using this method, we have a way to estimate the distortion present in an image. First, a set of polynomials is selected; a common set of polynomials to use is the Zernike set,³ but there are many others that can be used. Second, a coefficient list or “vector” of numbers is created; each number in this list will be the coefficient in front of its corresponding polynomial in the set of polynomials. This gives us a way to weight each of the polynomials in the set. Next, an algorithm is set up to change each number in the coefficient list, and, at each change, the point spread function is calculated (by the method above). This calculated, or estimated, point spread function is then compared to the observed point spread function, and an error metric is calculated. The algorithm will seek to minimize this error metric; once this is minimized, the calculated point spread will be quite similar to the observed point spread function. At this point, we know the distortion acting on the system; it is simply the set of polynomials, each weighted by its coefficient found by the algorithm.






Searching for the correct polynomials weighted by the correct coefficients is not trivial. Sometimes certain polynomials can be ignored if it is known by symmetry that they will not show up in the point spread function. Regardless, searching for the correct distortion is an optimization of a function in a huge parameter space. Typical algorithms use a steepest descent approach [Fie82], which changes one parameter at a time, calculates an error between that estimation and the observed point spread function, and seeks to minimize this error. There have also been algorithms that use random searches, Monte Carlo walks, and Markov chain Monte Carlo searches that claim robustness and speed [Fie82].

Once the correct distortion is calculated, the information is sent to the deformable mirror, which is where the term “adaptive optics” comes from. This mirror consists of many smaller mirrors, each of which can be precisely adjusted by a piezoelectric actuator. The mirror changes shape, creating a conjugate wavefront that the image from the telescope can be reflected off. At this point, the atmospheric distortion has been removed from the image. Normally, this is done in real time, and so speed of both the calculation algorithm and of the deformable mirror must be optimized. Systems typically can calculate and adjust in under a second [PW06].

³The Zernike set of polynomials described many optical distortions such as spherical aberration, defocus, coma, etc., and is chosen for systems displaying these distortions

Bibliography

- [CER] CERN. Spin polarization by optical pumping. <https://collaps.web.cern.ch/beta-nmr/spin-polarization>. Accessed: 12.11.2017.
- [Com] Wikipedia Commons. Veranschaulichung der präzession eines atomspins um ein externes magnetfeld. <https://commons.wikimedia.org/wiki/File:Pr%C3%A4zession2.png>. Accessed: 14.12.2017.
- [dD06] M.J.A de Dood. Second-harmonic generation: How to get from a wavelength of  to 490. *Huygens Laboratory*, 2006.
- [ESO] ESO. Laser guide star at the vlt. <https://www.eso.org/public/images/dsc1792-cc/>. Accessed: 4.12.2017.
- [Fey65] Richard Feynman. The hyperfine splitting in hydrogen. *California Institute of Technology*, 1965.
- [Fie82] James R. Fienup. Phase retrieval algorithms: a comparison. *Applied  Optics*, 21.15:2758–2769, 1982.
- [Gon82] R. A. Gonsalves. Phase retrieval and diversity in adaptive optics. *Optical Engineering*, 21.5:829 – 832, 1982.
- [JES97] S. G. Payton J. E. Sohl. A modular, reconfigurable cavity, pulsed dye laser for the advanced undergraduate laboratory. *American Journal of Physics*, 65.7:640–652, 1997.
- [JH01] A. Gregory J. Henry. Moving heaven and earth: Copernicus and the solar system. *Cambridge*, page 87, 2001. 
- [Kib09] E. Kibblewhite. The physics of the sodium laser guide star: Predicting and enhancing the photon returns. *Advanced Maui Optical and Space Surveillance Technologies Conference*, 2009.
- [KS77] T. Sikkeland K.A. Selanger, J. Farnes. Fluorescence lifetime studies of rhodamine 6G in methanol. *The Journal of Physical Chemistry*, 81.20:1960–1963, 1977.

- [NAS03] NASA. Telescope history. https://www.nasa.gov/audience/forstudents/9-12/features/telescope_feature_912.html, 09.12.03. Accessed: 12.11.2017.
-  [ps09] W. M. Keck Observatory. A short history of astronomy and telescopes, 2009.
- [Oko] Gabriel Okolski. A brief history of the hubble space telescope. 
- [Pri91]  al. Primmerman, Charles A. Compensation of atmospheric optical distortion using a synthetic beacon. *Nature*, 353.6340:141–143, 1991.
- [PW06]  H. Bouchez R. D. Campbell J. C. Y. Chin A. R. Contos M. A. van Dam S. K. Hartman E. M. Johansson R. E. Lafon P.L. Wizinowich, D.L. Mignant. The W.M. Keck observatory laser guide star adaptive optics system: Overview. *Astronomical Society of the Pacific*, 118:840, 2006.
- [RH10]  Bonaccini Calia D. Budker J. M. Higbie W. Hackenberg R. Holzlohner, S. M. Rochester. Optimization of CW sodium laser guide star efficiency. *Astronomy and Astrophysics*, 510, 2010.
- [RR15] S. M. Rochester R. Holzlohner R. Rampy, D. Gavel. Toward optimization of pulsed sodium laser guide star. *JOSA B*, 32.12:2425–2432, 2015.
- [SHG] Second harmonic generation. <https://staff.aist.go.jp/narazaki-aiko/SHG>. Accessed: 16.11.2017.
- [ST] Sky and Telescope. How to successfully beat atmospheric distortion. <http://www.skyandtelescope.com/astronomy-equipment/beating-the-seeing/>. Accessed: 15.11.2017.
- [Ste01] Daniel A. Steck. Rubidium 87 D line data. 2001.
- [Tec] Elent Technics. Acousto-optic modulators. <http://www.elent-a.net/index.php/en/products-2/teo2-crystals/acousto-optical-applications/acousto-optical-modulators>. Accessed: 8.12.2017.
- [TJK14] C. A. Denman T. J. Kane, P. D. Hillman. Pulsed laser architecture for enhancing backscatter from sodium. *International Society for Optics and Photonics*, 9148:3G, 2014.
- [Uni] Penn State University. Not just a laser pointer. <http://sites.psu.edu/howzscienceofmovies/2014/10/03/not-just-a-laser-pointer/>. Accessed: 15.11.2017.